Effect of radial plasma transport at the magnetic throat on axial ion beam formation

Yunchao Zhang, Christine Charles, and Rod Boswell

Citation: Physics of Plasmas **23**, 083515 (2016); doi: 10.1063/1.4960828
View online: http://dx.doi.org/10.1063/1.4960828
View Table of Contents: http://scitation.aip.org/content/aip/journal/pop/23/8?ver=pdfcov
Published by the AIP Publishing

Effect of radial plasma transport at the magnetic throat on axial ion beam formation

Yunchao Zhang,[a] Christine Charles, and Rod Boswell
Space Plasma, Power and Propulsion Laboratory, Research School of Physics and Engineering, The Australian National University, Bldg 60, Mills Road, Canberra, Australian Capital Territory 2601, Australia

(Received 11 June 2016; accepted 29 July 2016; published online 10 August 2016)

Correlation between radial plasma transport and formation of an axial ion beam has been investigated in a helicon plasma reactor implemented with a convergent-divergent magnetic nozzle. The plasma discharge is sustained under a high magnetic field mode and a low magnetic field mode for which the electron energy probability function, the plasma density, the plasma potential, and the electron temperature are measured at the magnetic throat, and the two field modes show different radial parametric behaviors. Although an axial potential drop occurs in the plasma source for both field modes, an ion beam is only observed in the high field mode while not in the low field mode. The transport of energetic ions is characterized downstream of the plasma source using the delimited ion current and nonlocal ion current. A decay of ion beam strength is also observed in the diffusion chamber. *Published by AIP Publishing.* [http://dx.doi.org/10.1063/1.4960828]

I. INTRODUCTION

Ion beams play an important role in electric propulsion systems[1] and materials processing.[2] Their formation along a divergent magnetic nozzle is closely associated with an axial potential drop which has been reported by both experiments[3–5] and theories.[6–8] However, the effect of radial plasma transport on ion beam formation has not been fully understood due to the complex cross-field phenomena of charged particles.[9–11] The present study aims at a better understanding of this problem, and unveils that radial confinement of ions at the magnetic throat is a necessary condition of axial ion beam formation.

II. EXPERIMENTAL SETUP

The experiment is carried out in the Chi-Kung reactor as shown in Figure 1(a) which, on the left hand side ($z < 0$ cm), consists of a cylindrical plasma source terminated with an aluminium earthed plate, and on the right hand side ($z > 0$ cm), a contiguously attached 30-cm long, 32-cm diameter, earthed aluminium diffusion chamber. The plasma source is made of a 31-cm long, 13.7-cm diameter Pyrex glass tube surrounded by an 18-cm long double saddle antenna operating at a constant power of 310 W at a radio frequency (RF) of 13.56 MHz. A turbo/primary pumping system is implemented to obtain a base pressure of 3×10^{-6} Torr in the reactor monitored with an ion gauge. Argon gas is fed to the system through a side wall port of the diffusion chamber at a constant gas pressure of 5×10^{-4} Torr measured with a Baratron gauge.

A solenoid close to the source exit is used to generate a convergent-divergent magnetic nozzle and the field lines calculated from the Biot-Savart law are shown in Figure 1(a) as solid curves. When a current generated from the direct-current (DC) power supply is transmitted into the solenoid, defined as the "solenoid current," it is divided equally into the two parallel coils due to the double-coil-wound arrangement. The magnetic flux density on the central axis ($B_z = B$) for a solenoid current of 9 A is measured by a gaussmeter in the range from $z = -25$ cm to 10 cm and the data, represented by open circles in Figure 1(b), show a maximum of 200 Gauss at $z = -9$ cm (location of the magnetic throat) and

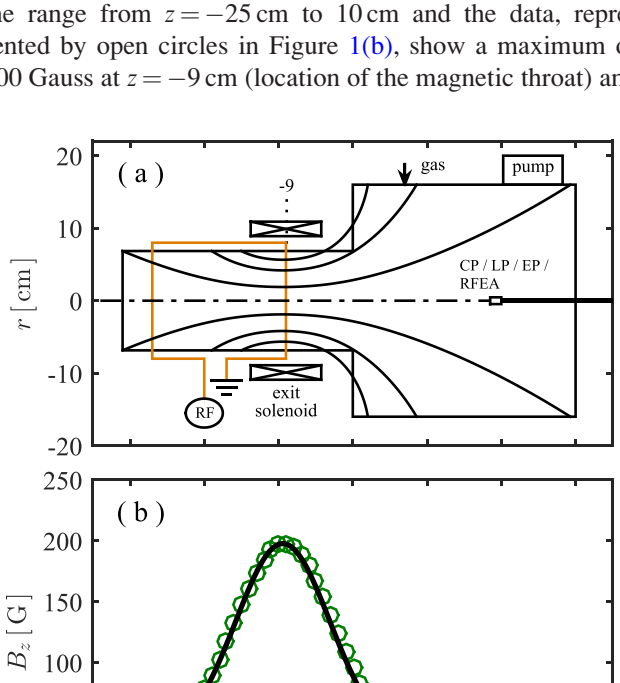

FIG. 1. (a) Chi-Kung reactor implemented with a convergent-divergent magnetic nozzle, showing the major components and diagnostic probes. The calculated field lines are plotted within the reactor geometry. (b) On-axis magnetic flux density generated with the solenoid current of 9 A, measured using a gaussmeter (open circles) and calculated from the Biot-Savart law (solid line), and calculated results for the solenoid current of 3 A (dashed line).

[a]yunchao.zhang@anu.edu.au

a symmetric decrease to tens of Gauss in the top region of the plasma source and in the diffusion chamber. Calculated results for the solenoid current of 9 A, represented by the solid line, are consistent with the gaussmeter measurements, and the results for a lower current of 3 A are given as the dashed line.

Four electrostatic probes are used as experimental diagnostics: a RF compensated Langmuir probe (CP), a planar Langmuir probe (LP), an emissive probe (EP), and a retarding field energy analyzer (RFEA), with their probe shafts and the reactor walls being grounded to a clean earth. A vacuum slide is mounted on the back plate of the diffusion chamber to allow positioning of the probes along both the axial and radial directions without breaking vacuum (except when changing the probe). The CP consisting of a 6-mm long, 0.25-mm diameter tungsten wire obtains the electron energy probability function (EEPF, in the form of $F_p(\epsilon_e, \xi)$, where ϵ_e and ξ are the electron kinetic energy and the spatial position, respectively) from the second derivative of the measured current-voltage trace (based on the Druyvesteyn theory[12,13]). The LP has a 1.9-mm diameter nickel tip and measures the ion saturation current I_{sat} at a negative bias voltage of -95 V. The EP consisting of a 0.2-mm diameter tungsten wire measures the plasma potential ϕ using the floating potential method. The RFEA consists of a structure with a 2-mm diameter orifice, four grids (an earthed grid, a repellor grid biased at -80 V, a discriminator grid, a secondary suppressor grid at -18 V) and a collector plate biased at -9 V, and gives the ion energy distribution function (IEDF) by differentiating the measured current-voltage curve $I_c(V_d)$. In the absence of an ion beam, the IEDF shows a single peak; in the presence of an ion beam, the IEDF exhibits a two-peak distribution and can be fitted by the sum of a low energy Gaussian function representing the background ion group and a high energy Gaussian function representing the ion beam.

III. RADIAL PLASMA TRANSPORT AT THE MAGNETIC THROAT

In order to characterize cross-field behaviors of electrons, the EEPFs are obtained at the magnetic throat at $z = -9$ cm (logarithmic scale on Figure 2), and for each mode, the curves are normalized by the maximum amplitude of on-axis data ($r = 0$ cm). With a strong magnetic field generated by a solenoid current of 9 A, the on-axis EEPF curve, represented by the solid line in Figure 2(a), shows a convex shape in the main energy range and beyond this an energetic tail starting at $\epsilon_e \sim 35$ eV which is masked by the experimental noise at the highest energy part. The EEPF measured at $r = -6$ cm (dashed line), close to the lateral wall of the source tube, presents a flattened curve shape compared to the on-axis data and its upper energy limit increases to about 80 eV. Figure 2(b) shows the EEPF measurements under a weak magnetic field generated by a solenoid current of 3 A. The on-axis EEPF presents a convex shape with an energetic tail over $\epsilon_e \sim 45$ eV similar to the 9 A case in Figure 2(a), and the EEPF at $r = -6$ cm exhibits a decrease in amplitude

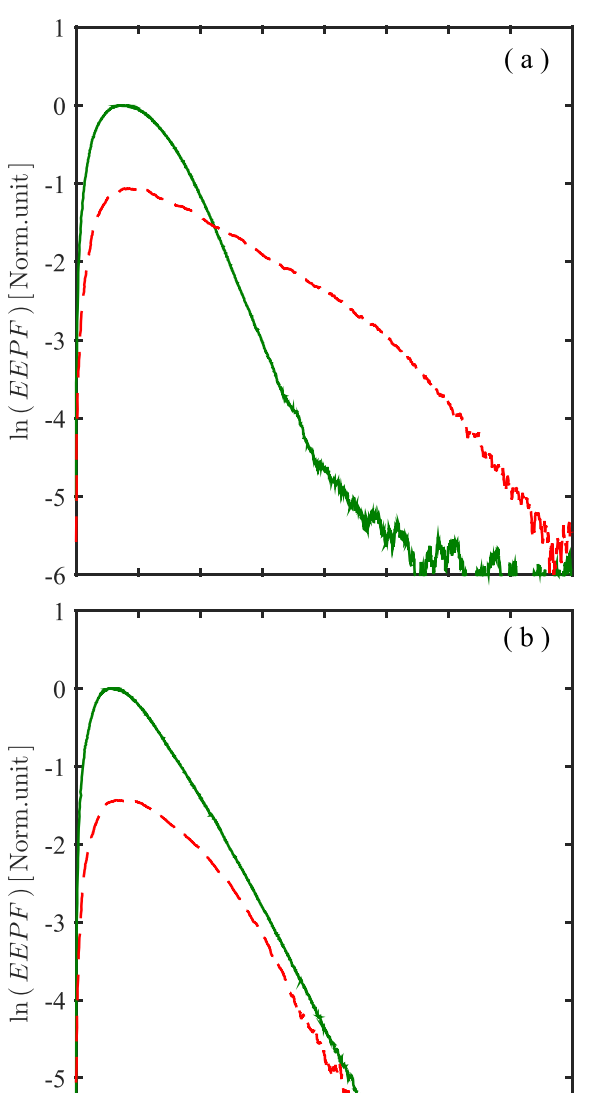

FIG. 2. Logarithm of normalized EEPFs for (a) high field mode with a solenoid current of 9 A and (b) low field mode with a solenoid current of 3 A, measured at $z = -9$ cm, $r = 0$ cm (solid line) and $r = -6$ cm (dashed line). The results are normalized by the maximum amplitude of EEPF curve measured on axis for each mode.

in the low energy range compared to the on-axis data and the upper energy limit remains unchanged.

These results suggest that there is a mode transition between the high magnetic field case and the low magnetic field case. The electrons are heated near the outer wall (due to skin heating effect near the RF antenna[14–16]) for the high magnetic field case with more high energy electrons located at $r = -6$ cm than at $r = 0$ cm (Figure 2(a)), while this heating mechanism is not identified for the low magnetic field case (Figure 2(b)). Auxiliary experiments have verified the magnetic-field-induced transition and a triggering solenoid current at about 4.5 A, below which the plasma discharge is defined as the low field mode and above (which) the high field mode. Since the EEPFs show a similar distribution pattern for different solenoid currents within each mode, the

typical cases of 9 A and 3 A are used to represent the high field mode and the low field mode, respectively. Previous studies have reported a similar transition occurring in a constant-divergent magnetic nozzle with a triggering mechanism shown to be the ion magnetization by using different source geometries.[17] It should be noted that a change in the conductivity of cross-field electrons could also result in a mode transition.[18]

The radial profile of electron (plasma) density at the magnetic throat ($z = -9$ cm) is calculated from the EEPF data using $n_e = \int_0^\infty \sqrt{\epsilon_e} F_p(\epsilon_e, \xi)\, d\epsilon_e$. The high field mode's density profile (open circles in Figure 3(a)) exhibiting a maximum of about $2.5 \times 10^{10}\,\mathrm{cm}^{-3}$ at $r = -5$ cm, combined with the hollow plasma potential profile (ϕ, obtained from the zero crossing of the second derivative of current-voltage traces) presenting a peak of 46.5 V at the same position in Figure 3(b), indicates that the plasma is sustained in the inductively coupled mode.[19,20] Both the density and plasma potential profiles for the low field mode (open triangles) show a peak on axis, with a density of about $6 \times 10^{10}\,\mathrm{cm}^{-3}$ and a potential of 42.5 V, likely due to an additional wave mode[20] which is consistent with a higher density measured for the low field mode compared to the high field mode. Experiments carried out in the annular Chi-Kung reactor[21] also support this scenario as no density rise in the inner region was observed for the low solenoid current case in the annular system. The maximum values in the potential and density profiles at about $r = -5$ cm in the high field mode suggest that a higher ion production rate occurs in the edge region compared to the central region, and this is consistent with the EEPFs in Figure 2 where more high energy electrons are located at $r = -6$ cm (dashed line) compared to $r = 0$ cm (solid line). Hence, the ions are well confined in the central region by a peripheral "potential barrier" and not lost onto the lateral wall. This ion confinement scenario does not exist in the low field mode where centrally peaked density and potential profiles result in radially outward motion of ions.

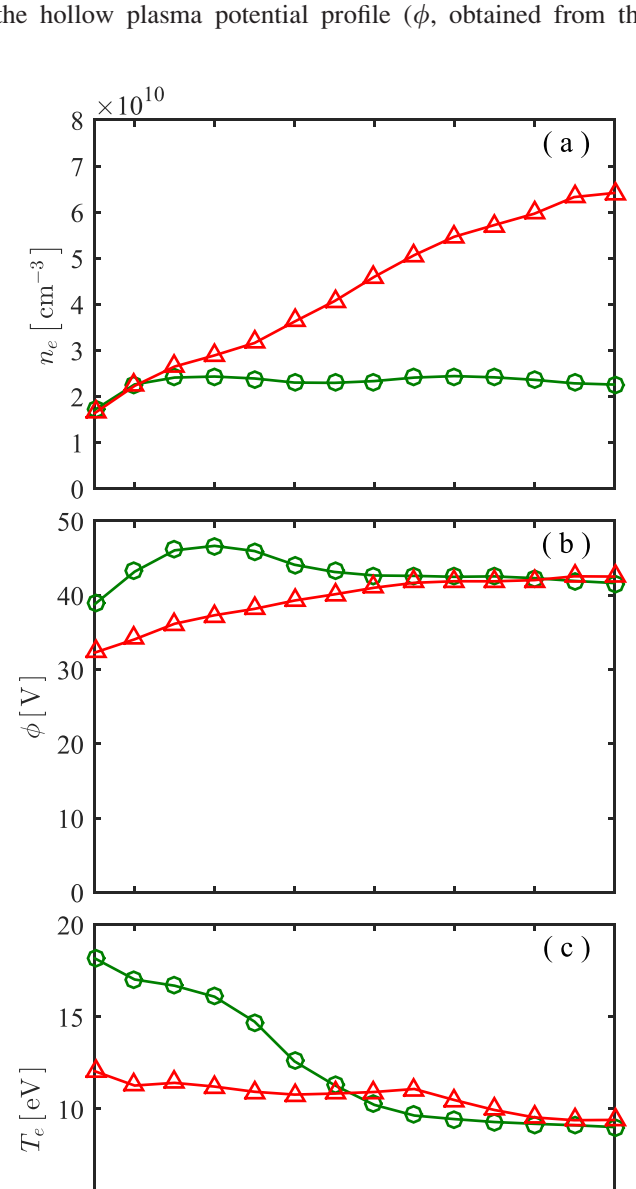

FIG. 3. Radial profiles of (a) electron (plasma) density n_e, (b) plasma potential ϕ, and (c) effective electron temperature T_e, measured at $z = -9$ cm for high field mode (open circles) and low field mode (open triangles).

The average kinetic energy of electrons is represented by the effective electron temperature defined as $T_e = \frac{2}{3n_e}\int_0^\infty \epsilon_e \sqrt{\epsilon_e} F_p(\epsilon_e, \xi)\, d\epsilon_e$. Its radial profile for the high field mode, represented by open circles in Figure 3(c), keeps relatively constant in the region of -3 cm $< r < 0$ cm and starts to increase at about $r = -4$ cm. The increase in electron temperatures is consistent with the results in Figure 2(a) where the EEPF curve is flattened at $r = -6$ cm compared to that at $r = 0$ cm. Similar phenomena have been observed in the helicon double layer thruster (HDLT) experiment[15] and magnetic filter experiment.[22] The low field mode also presents increasing electron temperatures along the radial direction (open triangles) but with a smaller gradient compared to the high field mode, as it is solely caused by the decrease of EEPF amplitude in the low energy range (without extending the upper energy limit) which effectively increase the average electron energy (Figure 2(b)).

The electron temperature has a positive correlation with the ionization rate and hence its behavior is a good indicator of particle balance within the plasma cavity.[2] Since the electron Larmor radius is much smaller than the ion Larmor radius, the electrons can be considered as independent micro-discharges along different magnetic field lines, while the ions are less magnetized and move across the magnetic field more freely. Each electron group should guarantee the balance of ions created nearby and ion flux loss in both parallel-to-field and cross-field directions. The parallel-to-field balance can be explained by the principle of L-p similarity,[23,24] where "L" is the length of magnetic field lines terminated by the source wall and "p" is approximately a constant for weakly ionized plasmas (with negligible neutral depletion[25,26]). The electron temperature is negatively correlated to "$L \times p$," and hence, it is larger on the short magnetic field lines close to walls than that on the long field lines in the central region.

The cross-field particle balance behaves differently under the two field modes. For the high field mode, electrons gain energy from skin heating near the source tube wall (Figure 2(a)) which results in enhanced impact ionization. Correspondingly, the plasma density and potential profiles (Figures 3(a) and 3(b)) exhibit maximum values (with a very definite peak in potential) at about $r = -5$ cm and the newly created ions will move in both outward and inward radial directions. For the low field mode, the ionization behavior changes (more ions being produced in the central region) with both the density and potential profiles decreasing from the central axis to the edge, thereby generating one-directional ion loss in the outer region (at about $r = -5$ cm) towards the source wall. These results are consistent with the larger electron temperature gradient measured in the outer region for the high field mode compared to the low field mode as shown in Figure 3(c).

IV. AXIAL ION BEAM FORMATION

The plasma shows different radial transport behaviors between the two field modes and it is of great interest to check their effects on the ion dynamics along the magnetic nozzle. The on-axis profile of ion (plasma) density n_i, measured by the LP and calculated using Sheridan's method,[27] is shown in Figure 4(a). The high field mode (open circles) presents a profile well following the magnetic intensity (Figure 1(b)) and has its maximum of about $3 \times 10^{10}\,\mathrm{cm}^{-3}$ at the magnetic throat at $z = -9$ cm. The low field mode (open triangles) exhibits its maximum of about $6 \times 10^{10}\,\mathrm{cm}^{-3}$ at $z = -15$ cm, close to the middle of the RF antenna, which is related to the possible wave mode in the central region. The ion density measured by the LP is in reasonable agreement with the electron density obtained from the CP. The axial profile of plasma potential obtained from the EP is given in Figure 4(b) and shows a consistent trend with the respective density profile, with a maximum potential of 41 V at $z = -9$ cm for the high field mode and of 43.5 V at $z = -15$ cm for the low field mode. If the ion transport was considered as a one-dimensional phenomenon, an ion beam should be observed in the diffusion chamber for both field modes due to the potential drop in the plasma source.

However, in Figure 5, the IEDF data (with respect to the discriminator voltage V_d and its amplitude being normalized for clarification) measured at $z = 7$ cm, $r = 0$ cm show an unexpected result. The high field mode (Figure 5(a)) presents a two-peak IEDF, i.e., an ion beam forms out of the plasma source, while the low field mode (Figure 5(b)) exhibits a single-peak distribution with a negligible tail (resolved in the inset), i.e., no ion beam is detected. A detailed description of ion transport from the plasma source into the diffusion chamber needs two-dimensional modeling of plasma dynamics in the magnetic nozzle and is related to a coupled ionization term between the radial and axial dimensions, which is beyond the scope of this study. Here, the radial behavior of high energy ions is simply reflected by the radial profile of delimited ion current I_{del} at $z = 1$ cm just downstream of the plasma source (shown in Figure 6(a)), defined as the RFEA-measured collector current at a chosen high discriminator voltage of 40 V which corresponds to the plasma potential at the magnetic throat for both field modes (Figure 4(b)), i.e., $I_{del} = I_c(V_d = 40\,\mathrm{V})$. The high field mode (represented by open circles) shows a maximum I_{del} near the central axis, as a result of the radial ion confinement in the plasma source discussed in Section III. For the low field mode (open triangles), the profile presents a lower magnitude compared to the high field mode which indicates that only a small portion of high energy ions are accelerated from the plasma source into the diffusion chamber, as a result of the ion loss towards the lateral source wall (discussed in Section III). Additionally, the higher magnetic field intensity for the high field mode is positively correlated to the ion confinement in the central region.

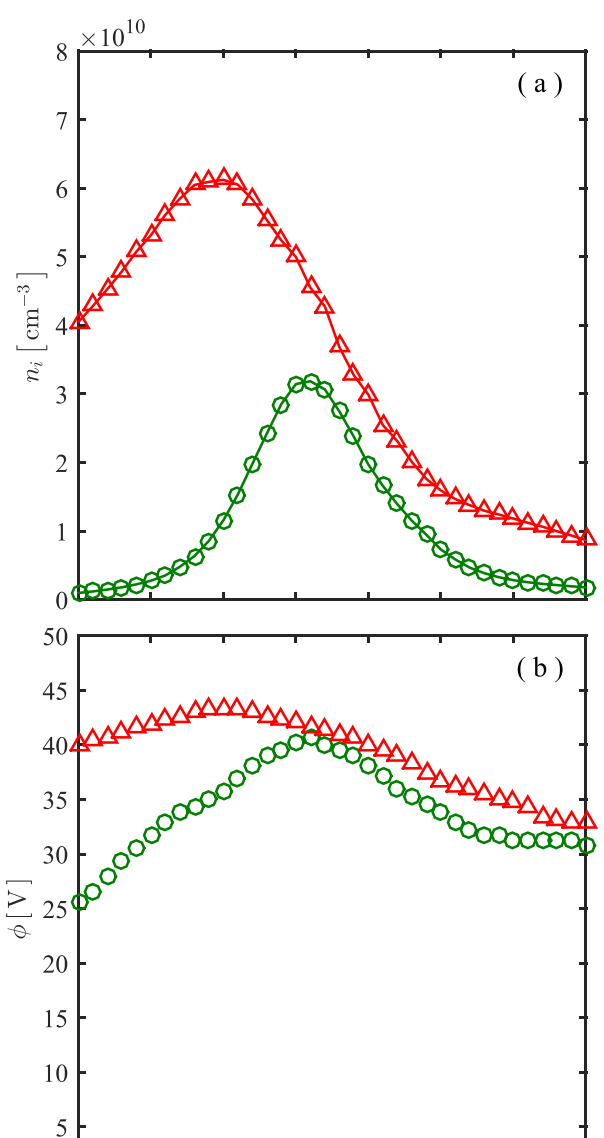

FIG. 4. Axial profiles of (a) ion (plasma) density n_i and (b) plasma potential ϕ, measured along $r = 0$ cm for high field mode (open circles) and low field mode (open triangles).

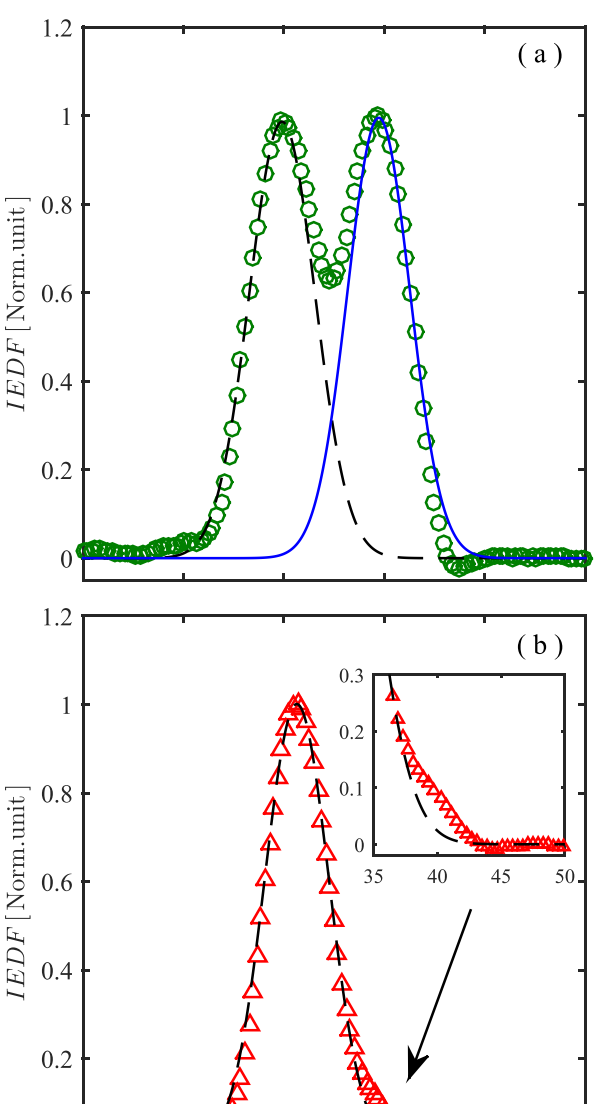

FIG. 5. Normalized IEDF curves measured at $z = 7$ cm, $r = 0$ cm for (a) high field mode, fitted by the sum of a low energy Gaussian function (dashed line) and a high energy Gaussian (solid line), and for (b) low field mode, fitted with a Gaussian function (dashed line) to the low energy part.

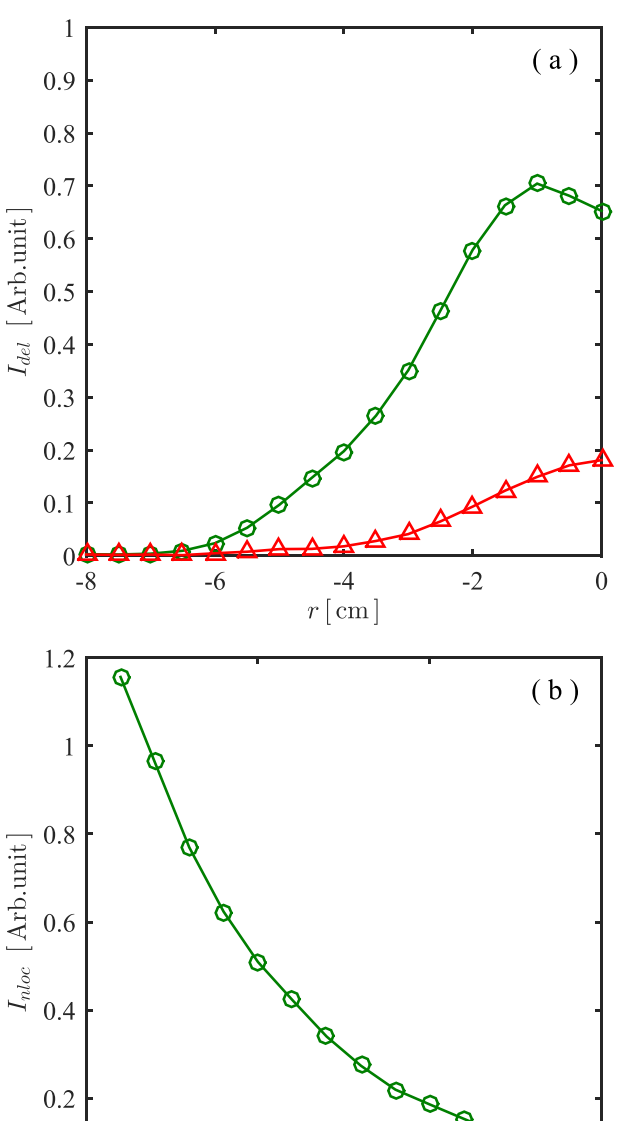

FIG. 6. (a) Radial profiles of delimited ion current I_{del} at $z = 1$ cm and (b) on-axis profiles of nonlocal ion current I_{nloc}, for high field mode (open circles) and low field mode (open triangles).

The on-axis transport of an ion beam in the diffusion chamber is not affected by the magnetic field and its variation on axis can be characterized by tracing the nonlocal ion group accelerated from the plasma source, which is represented by the nonlocal ion current I_{nloc} derived from integral of the high energy Gaussian function (solid line) fitted to the high-field-mode IEDF in Figure 5(a). Correspondingly, a local ion current I_{loc} representing the background ion group around the RFEA is given by integral of the low energy Gaussian function (dashed line), as previously reported in Ref. 21. For the low field mode (Figure 5(b)), the IEDF can only be fitted with a Gaussian function (dashed line) to the low energy part which yields the local current. The nonlocal component contributed by the small energetic tail is given by subtracting the local current (I_{loc}) from the total ion current I_{tot} (integral of the overall IEDF). The on-axis profile of nonlocal ion current obtained from $z = 1$ cm to 15 cm is given in Figure 6(b) and shows higher values for the high field mode (open circles) compared to the low field mode (open triangles). The ion beam of the high field mode decays along the axial direction due to plasma expansion in the diffusion chamber and ion-neutral collisions.

V. SUMMARY

This study shows that ion beam formation along a divergent magnetic nozzle is not a one-dimensional phenomenon solely determined from the axial potential drop and it is correlated with the radial confinement of ions at the magnetic throat. For the high field mode, high energy electrons are located near the source tube wall with enhanced ionization

due to skin heating effect; the radial profiles of plasma density and potential create a peripheral potential barrier confining the ions. Consequently, an axially focused ion beam forms. For the low field mode, the ionization mechanism changes and more ions are created in the central region, resulting in an outward motion of ions from the central region towards the radial edge. In this configuration, no ion beam is detected downstream of the plasma source although an axial potential drop (similar to that for the high field mode) exists. These results could be applied to improve the propellant efficiency of electric thrusters and to optimize the system design of focused ion beam devices.

[1]D. M. Goebel and I. Katz, *Fundamentals of Electric Propulsion: Ion and Hall Thrusters*, JPL Space Science and Technology Series (John Wiley and Sons, New York, 2008).
[2]M. A. Lieberman and A. J. Lichtenberg, *Principles of Plasma Discharges and Materials Processing*, 2nd ed. (John Wiley and Sons, New York, 2005).
[3]C. Charles and R. W. Boswell, "Current-free double-layer formation in a high-density helicon discharge," Appl. Phys. Lett. **82**, 1356 (2003).
[4]X. Sun, A. M. Keesee, C. Biloiu, E. E. Scime, A. Meige, C. Charles, and R. W. Boswell, "Observations of ion-beam formation in a current-free double layer," Phys. Rev. Lett. **95**, 025004 (2005).
[5]A. Fredriksen, L. N. Mishra, and H. S. Byhring, "The effects of downstream magnetic field on current-free double layers and beam formation in the njord helicon plasma device," Plasma Sources Sci. Technol. **19**, 034009 (2010).
[6]W. M. Manheimer and R. F. Fernsler, "Plasma acceleration by area expansion," IEEE Trans. Plasma Sci. **29**, 75 (2001).
[7]A. Fruchtman, "Electric field in a double layer and the imparted momentum," Phys. Rev. Lett. **96**, 065002 (2006).
[8]A. V. Arefiev and B. N. Breizman, "Ambipolar acceleration of ions in a magnetic nozzle," Phys. Plasmas **15**, 042109 (2008).
[9]A. P. Zhilinskii and L. D. Tsendin, "Collisional diffusion of a partially-ionized plasma in a magnetic field," Sov. Phys. Usp. **23**, 331 (1980).
[10]P. Chabert and N. Braithwaite, *Physics of Radio-Frequency Plasmas* (Cambridge University Press, Cambridge, 2011).
[11]D. Curreli and F. F. Chen, "Cross-field diffusion in low-temperature plasma discharges of finite length," Plasma Sources Sci. Technol. **23**, 064001 (2014).
[12]N. Hershkowitz, "How langmuir probes work," in *Plasma Diagnostics*, Plasma-Materials Interactions, Vol. 1, edited by O. Auciello and D. L. Flamm (Academic Press, Inc., 1989), Chap. 3, p. 113.
[13]V. A. Godyak, R. B. Piejak, and B. M. Alexandrovich, "Probe diagnostics of non-maxwellian plasmas," J. Appl. Phys. **73**, 3657 (1993).
[14]M. H. Lee and S. W. Choi, "Evolution of an electron energy distribution function in a weak dc magnetic field in solenoidal inductive plasma," J. Appl. Phys. **104**, 113303 (2008).
[15]K. Takahashi, C. Charles, R. W. Boswell, and R. Hatakeyama, "Radial characterization of the electron energy distribution in a helicon source terminated by a double layer," Phys. Plasmas **15**, 074505 (2008).
[16]S. H. Song, Y. Yang, P. Chabert, and M. J. Kushner, "Electron energy distributions in a magnetized inductively coupled plasma," Phys. Plasmas **21**, 093512 (2014).
[17]K. Takahashi, C. Charles, R. W. Boswell, and T. Fujiwara, "Double-layer ion acceleration triggered by ion magnetization in expanding radiofrequency plasma sources," Appl. Phys. Lett. **97**, 141503 (2010).
[18]M. Mitchner and C. H. Kruger, *Partially Ionized Gases*, Wiley series in plasma physics (John Wiley and Sons, New York, 1973).
[19]J. Hopwood, C. R. Guarnieri, S. J. Whitehair, and J. J. Cuomo, "Langmuir probe measurements of a radio frequency induction plasma," J. Vac. Sci. Technol. A **11**, 152 (1993).
[20]C. Charles, "Plasmas for spacecraft propulsion," J. Phys. D: Appl. Phys. **42**, 163001 (2009).
[21]Y. Zhang, C. Charles, and R. W. Boswell, "Characterization of an annular helicon plasma source powered by an outer or inner rf antenna," Plasma Sources Sci. Technol. **25**, 015007 (2016).
[22]A. Aanesland, J. Bredin, P. Chabert, and V. Godyak, "Electron energy distribution function and plasma parameters across magnetic filters," Appl. Phys. Lett. **100**, 044102 (2012).
[23]D. D. Monahan and M. M. Turner, "On the global model approximation," Plasma Sources Sci. Technol. **18**, 045024 (2009).
[24]S. Chatterjee, S. Bhattacharjee, C. Charles, and R. W. Boswell, "Electron energy probability function and l-p similarity in low pressure inductively coupled bounded plasma," Front. Phys. **3**, 7 (2015).
[25]A. W. Degeling, T. E. Sheridan, and R. W. Boswell, "Intense on-axis plasma production and associated relaxation oscillations in a large volume helicon source," Phys. Plasmas **6**, 3664 (1999).
[26]A. Fruchtman, G. Makrinich, P. Chabert, and J. M. Rax, "Enhanced plasma transport due to neutral depletion," Phys. Rev. Lett. **95**, 115002 (2005).
[27]T. E. Sheridan, "How big is a small langmuir probe?" Phys. Plasmas **7**, 3084 (2000).